Electronic Supplementary Material (ESI) for Nanoscale
This journal is © The Royal Society of Chemistry 2014

Supporting Information for:

Self-Organization and nanostructural control in thin film heterojunctions

Sebastiano Cataldo,[a] Camillo Sartorio,[a] Filippo Giannazzo,[b] Antonino Scandurra[c] and Bruno Pignataro*[a]

[a] Dipartimento di Fisica e Chimica, Università degli Studi di Palermo, V.le delle Scienze, Ed.17 – 90100 Palermo (Italy); E-mail: bruno.pignataro@unipa.it
[b] CNR-IMM, Strada VIII, 5 - 95121 Catania (Italy)
[c] CCR-SuperLab c/o STMicroelectronics; Strada VIII, 5 - 95121 Catania (Italy)

Table of Contents:

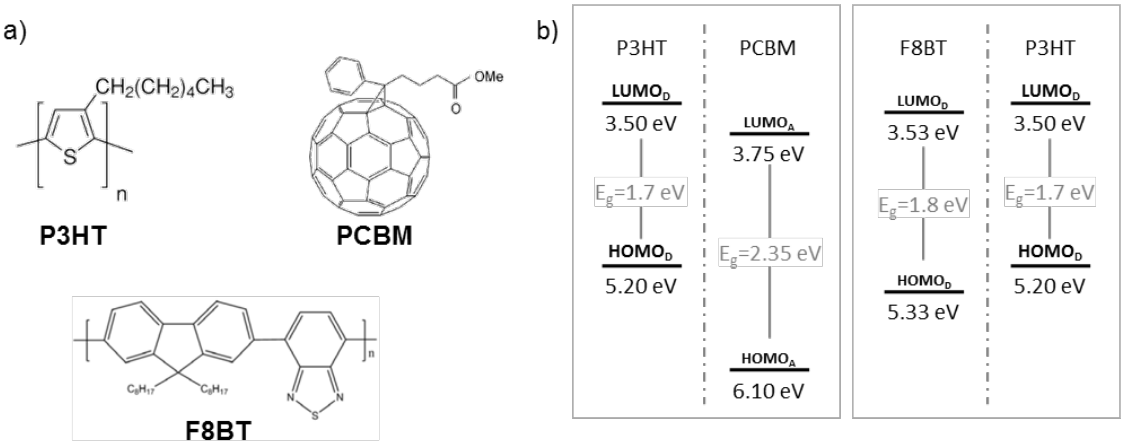

Figure S1: Chemical structures and energy band diagrams of materials used in experiments.

1. Surface Energy Measurements

Surface free energy of P3HT and F8BT thin-films consisting of three layers deposited by LS, have been calculated through the van Oss-Chaudhury-Good approach[1, 2] on the basis of contact angles measured by the sessile drop method.

Contact angles of ultrapure water (Millipore Milli-Q, 18.2 MΩ·cm), glycerol (Aldrich, 99%) and tritolyl-phosphate (Aldrich, 90%), have been measured at room temperature using a Kernco G-II Stage apparatus, by depositing on the surfaces of P3HT and F8BT samples 5 µl drops of these liquids. Table S1 report the average contact angle, calculated on five measurements on as many points on the surface.

Substance	F8BT	P3HT
Water	95°	95°
Glycerol	86°	94°
Tritolyl-	55°	72°

Table S1: Contact angle data measured on F8BT and P3HT surfaces.

By applying the van Oss-Chaudhury-Good algorithm for the substances in Table S1, we have employed the following Lifshitz-Van der Waals (γ^{LW}), acid-base (γ^{-}; γ^{+}) and total ($\gamma^{tot} = \gamma^{LW} +$

$2(\gamma^{-}\gamma^{+})^{1/2}$) surface energy values[3] (see Table S2) to calculate the P3HT and F8BT thin-film surface free energy.

Substance	γ^{LW}	γ^{-}	γ^{+}	γ^{tot}
Water	21.8	25.5	25.5	72.8
Glycerol	34.0	57.4	3.9	64.0
Tritolyl-phosphate	40.9	0	0	40.9

Table S2: Surface energy values employed in the surface free energy calculation, expressed in mJ/m^2.

The resulting surface free energy values for P3HT and F8BT were:

$\gamma_{P3HT} = 17.5\ mJ/m^2$

$\gamma_{F8BT} = 26.0\ mJ/m^2$

2. Atomic Force Microscopy (AFM)

The surface morphology of thin films was investigated by using an AFM microscope (Nanoscope IIIa, Veeco, Santa Barbara, CA) equipped with an extender electronics module in tapping mode. Etched-silicon probes (RTESP-type, Veeco) with a pyramidal-shape tip having a nominal curvature of 10 nm and a nominal internal angle of 35° were used. During the scanning, the cantilever (125 µm in length), with a nominal spring constant in the range of 20–100 N/m, was oscillating at its resonance frequency of about 330 kHz. Height and phase images were recorded simultaneously by collecting 512 × 512 points for each scan and maintaining the scan rate below 1 line per second.

2.1. AFM Thickness Measurements

The thickness of thin films has been measured by the scratching method. This consists in roughly pressing the AFM tip against the surface (6-8 V applied set-point; 30 Hz scan rate) during three consecutive scan to completely remove the material. Thus, the film thickness is determined from the section analysis of the carved scratch (Figure S2).

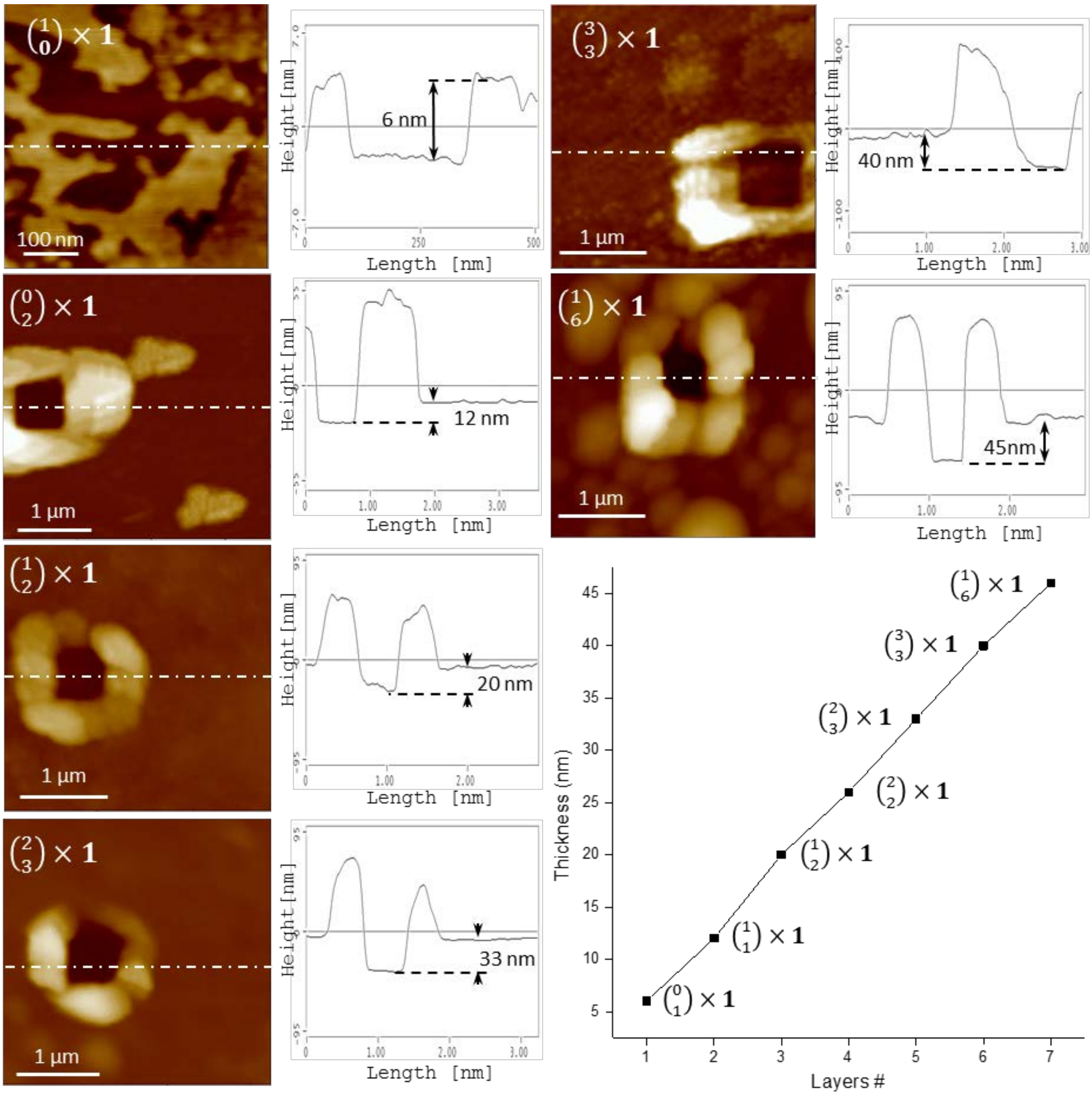

Figure S2: AFM thickness measurements of various P3HT:PCBM MHJs with aside the relative section analyses along the lines marked in the images. In the bottom-right panel, a graph of thickness vs. MHJ layers shows a linear trend.

2.2. Thin-film section by AFM

AFM section images (Figure S3**)** has been recorded on thin-films deposited on Silicon plates, by using a special support (Veeco Instruments) to vertically place the sample under the AFM tip. After the preparation, sample was cut by cleaving the silicon in order to expose a fresh section surface. The figure shows the section morphology of a P3HT:PCBM $\binom{3}{3}$ x4 MHJ.

However, the annealed film show a consistent thickness of 200 nm. The as-deposited MHJ film displays a smooth vertical morphology and it is possible to glimpse the layered structure. After the thermal annealing, the vertical morphology changes appearing phase-separated and showing round domains of about 10-20 nm in size.

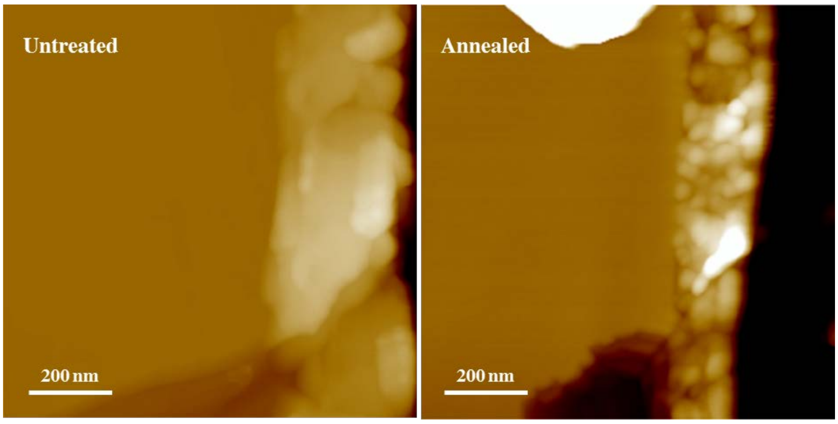

Figure S3: AFM section morphology of a P3HT:PCBM $\binom{3}{3}$ x4 MHJ: a) as deposited; b) annealed at 130°C 20min.

2.3. AFM Morphology

Figure S4a,b displays the AFM analysis of one P3HT LS layer characterized by a network structure. By transferring one layer of PCBM on top of the P3HT layer, figure S4c,d shows its typical granular morphology.[4] As expected, the PCBM layer covers densely and quite uniformly the P3HT layer without significant alteration since one can still recognize the P3HT network structure underneath.

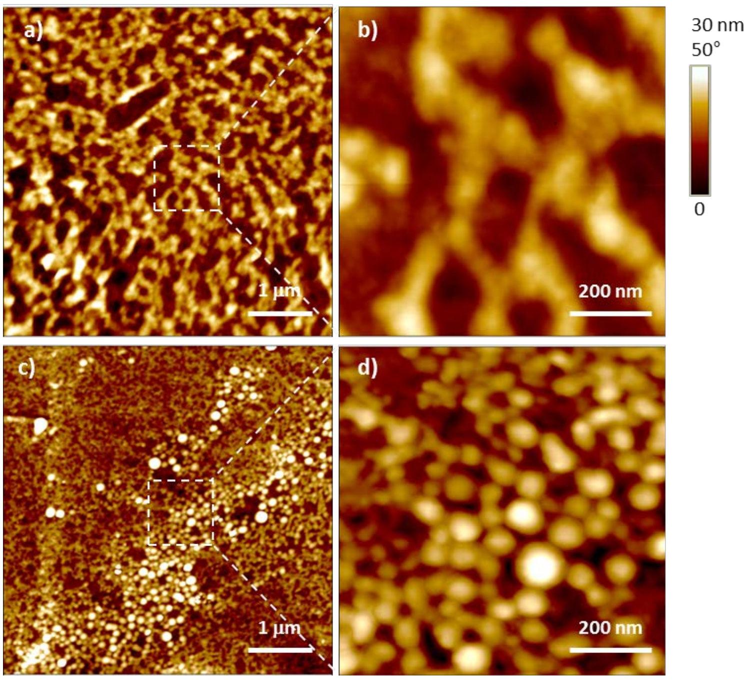

Figure S4: AFM images of (a,b) P3HT film and (c,d) $\begin{pmatrix}1\\1\end{pmatrix} \times 1$ P3HT:PCBM MHJ on ITO/PET; a,c) Height images; b,d) zoom-in of the region marked in a,c).

This above, together with other observations during the fabrication steps of others MHJs (Figure S5), shows that sequentially deposited layers retain their own structure and lie steadily at ambient temperature one on top of the other in the MHJ.

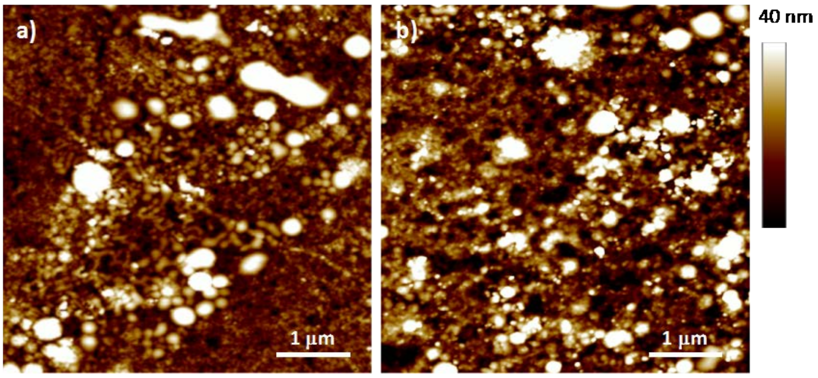

Figure S5: AFM morphology of P3HT:PCBM MHJs with architectures: a) $\begin{pmatrix}2\\2\end{pmatrix}$ x1; b) $\begin{pmatrix}3\\3\end{pmatrix}$ x1.

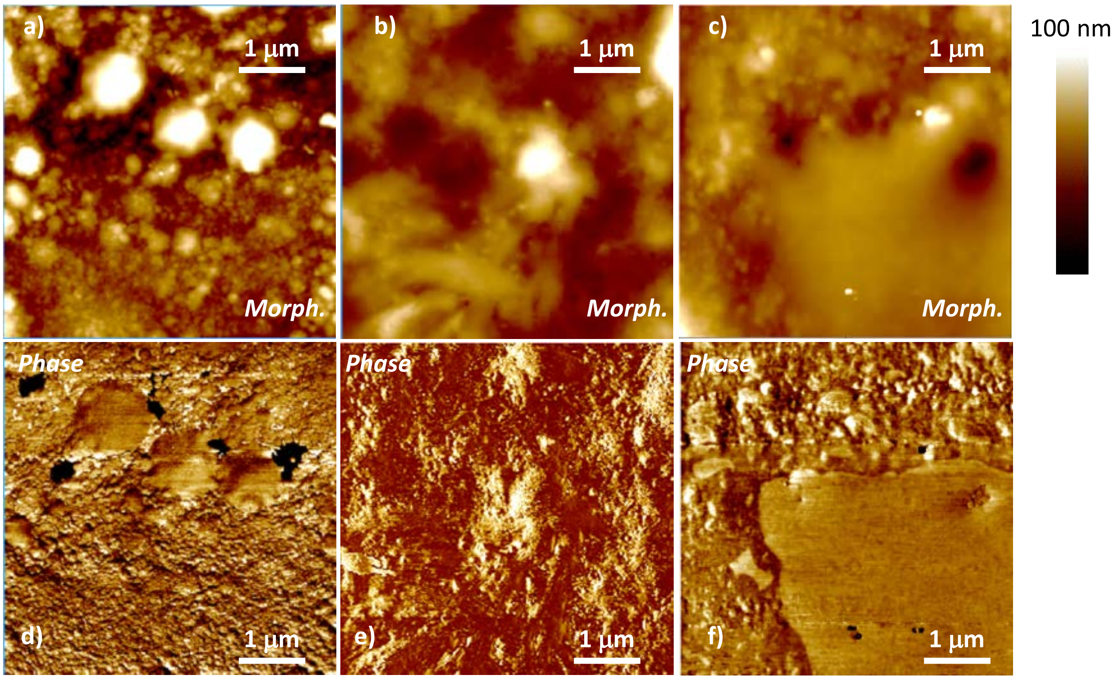

Figure S6: AFM surface analysis of a $\binom{3}{3} \times 2$ P3HT:F8BT MHJ films on ITO/PET at different annealing time and temperatures: a,d) non-annealed; b,e) 130°C, 15 min; c,f) 220°C, 30 minutes; a-c) height images; d-f) phase-lag images.

By employing a $\binom{3}{3} \times 2$ P3HT:F8BT MHJ, Figure S6 shows a behavior similar to the P3HT:PCBM blend upon thermal treatment for such a system. Also in this case, the stronger is the annealing treatment the smoother is the surface, its roughness decreasing from about 14 nm (Figure S6a, untreated sample) to about 10 nm (Figure S6b; 130°C, 15 min), up to about 6 nm (Figure S6c; 220°C, 30 min). In parallel, the phase-lag images show a quite uniform low contrast F8BT layer before annealing (Figure S6d), whereas bright-contrasting plaques (Figure S6c,f) appear upon annealing probably due to the topmost segregation of P3HT.

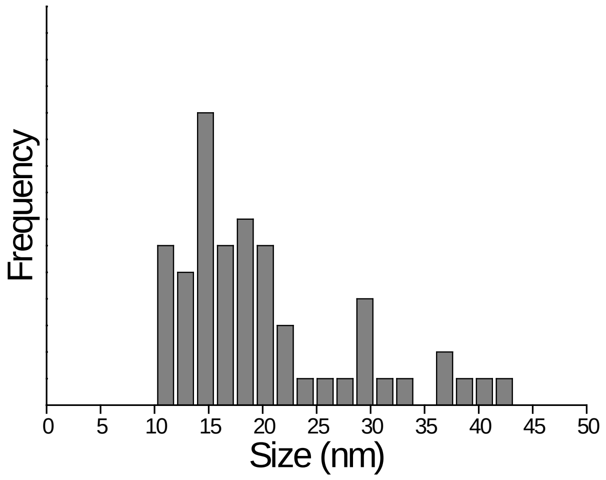

Figure S7: Size distribution histograms of dark domains in AFM phase-lag image of figure 1f.

2.4. Conductive AFM

The local electrical properties of the heterojunctions were investigated by Conductive Atomic Force Microscopy (C-AFM) under ambient conditions (50% humidity and 25°C) by means of a Dimension Nanoscope V (Veeco Instruments Inc., Santa Barbara, California) equipped with a Tunnelling AFM (TUNA) module. The current maps were obtained in contact regime using Pt/Ir coated tips (Veeco probes, SCM-PIC type) having a spring constant of 0.2N/m.

Referring to the figure 2 in the paper, the curves recorded after the annealing within the dark domains (figure 2f) show a higher slope than the bright regions (figure 2g), both in positive and negative curve branches. Since the IV curve slope is inversely related with the differential resistance[5] of the semiconductive thin film, this behaviour agrees with the formation of vertical conductive pathways with reduced resistance and with a current map showing contrast in contact resistance and charge mobility as expected in BHJ thin films made of two different component phases. The dashed lines mark the bias at which the current maps were acquired (-3 V), highlighting the greater current output from the dark domains in the annealed sample. Still, the sharp switch-on points at high voltages are indicative of the injection limited transport.

Besides, it is well-known that C-AFM maps give local information on the Schottky barrier at the tip-surface (metal-semiconductor) interface. In accordance with the Schottky-Mott rule,[6] which has been demonstrate to be valid also for organic semiconductors,[7] the Schottky barrier height (E_S) is the difference between the metal work function (ϕ) and the semiconductor electron affinity (χ; the LUMO level): $E_S = \phi - \chi$. Additionally, the Schottky barrier height is directly related to the switch-on voltage then, the lower is the switch-on voltage the higher is the electron affinity. Therefore it is possible to conclude that black domains, which are characterized by the lowest switch-on potential, would be mainly composed by the highest electron affinity component (lowest LUMO) that is the PCBM (see energy bands diagram in figure S1b).

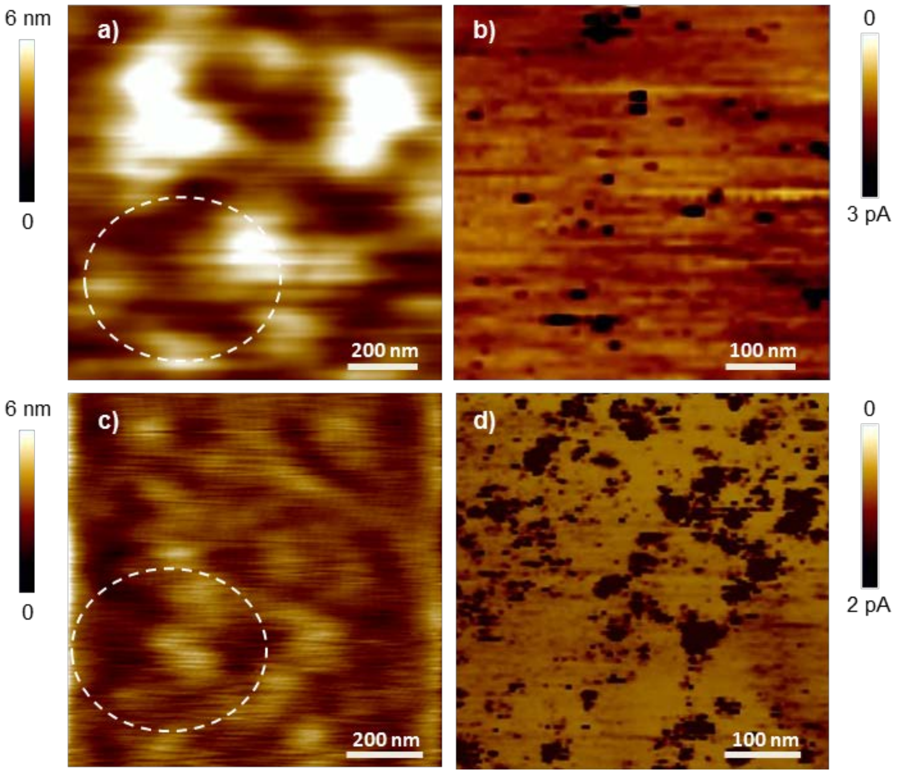

Figure S8: C-AFM surface analysis of a $\binom{3}{3} \times 2$ P3HT:PCBM MHJ; a,b) non-annealed sample; c,d) annealed at 130 °C for 10 min. a,c) height images; b,d) current maps acquired in the region marked in a,c panels.

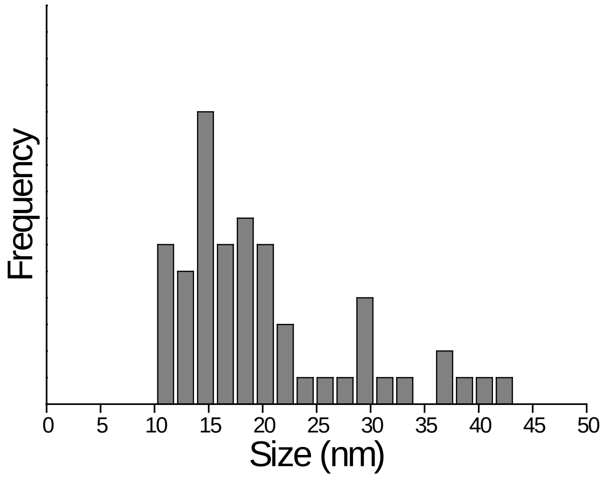

Figure S9: Size distribution histograms of dark domains in the C-AFM image of figure 2d.

3. Spectroscopic analysis

3.1. Photoelectron Spectroscopy

X-ray Photoelectron Spectroscopy (XPS) characterization has been obtained by using a Kratos AXIS-HS Spectrometer. Radiation Al Kα of 1486.6 eV has been used at the conditions of 10 mA and 15 keV. Areas of 2 mm × 2 mm have been analysed. The pass energy of 40 eV has been used both for survey and high resolution spectra. The binding energy scale was referred to the lowest binding energy component in the C1s spectra fixed at 284.7 eV. During the analysis the base pressure in the chamber was of the order of 10^{-7} Pa. Spectra fitting have been done after linear background subtraction by using VISION Software (Version 1.4.0) by Kratos Analytical.

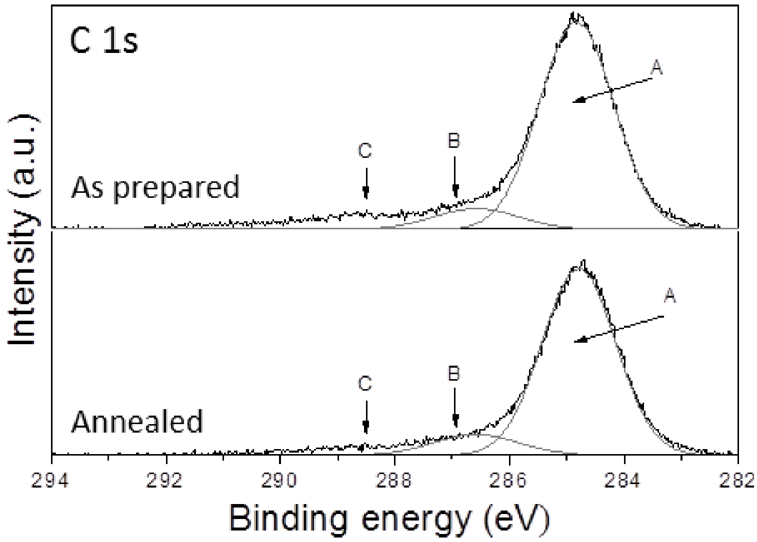

Figure S10: XPS spectra of the C_{1s} spectral regions for a $\binom{3}{3} \times 2$ P3HT:PCBM MHJ, before and after annealing at 130°C for 10 min.

In Figure S10, the spectrum of the as deposited sample shows three main features: a main peak (A) centered at about 284.7 eV which can be attributed to chemical groups such as (C=C)-H of PCBM; a less intense component (B) centered at about 286.5 eV assigned to C-O groups coming from slight PCBM surface oxidation; a bump (C) that can be assigned to shake up coming from π^*-π transitions in the C_{60} groups. Due to low concentration of carbon atoms of the ester group, compared to the total carbon atoms of PCBM, the corresponding components in the C1s spectrum are indistinguishable from that of oxidized carbon. The spectrum of annealed sample is similar to the previous described, being the BE of the component coming from C=C-H groups in the P3HT very close to that coming from PCBM then not resolved in our conditions. Once again a less intense component (B) due to slight surface oxidation is observed. Noteworthy, the C_{60} shake-up component (C) is less pronounced after the thermal annealing that is probably a consequence of the PCBM sinking. This further support the interdiffusion of the MHJ layers on the way to BHJ formation.

P3HT:F8BT	**C%**	**O%**	**N%**	**S%$_{\mathbf{F8BT}}$**	**S%$_{\mathbf{P3HT}}$**
As deposited	90.4	2.8	5.3	1.3	0.2
Annealed 130°C	91.3	3.8	3.3	1.14	0.4

Table S3: XPS atomic percentage for a P3HT:F8BT $\binom{3}{3} \times 2$ MHJ before and after a thermal annealing of 30 minutes at 130°C.

Table S3 reports the atomic percentage recorded at sample surface by XPS for a P3HT:F8BT $\binom{3}{3} \times 2$ MHJ before and after a thermal annealing of 30 minutes at 130°C. Shown data, demonstrate that after the annealing treatment the surface amount of the diazole nitrogen that is contained only in the F8BT is almost halved. This suggests that also in this case, P3HT is migrating at the surface whereas F8BT is sinking inside the film indicating that F8BT is sinking inside the film.

3.2. Optical Spectrophotometry

Absorption and fluorescence spectra were recorded on freshly prepared thin films of about t 80 nm on thickness, with a Specord S 600 spectrophotometer (Analytik Jena, Jena, Germany) and a Fluoromax-4 (HORIBA Jobin Yvon, Edison, USA) spectrofluorimeter with 150 W xenon arc lamp excitation source, respectively. The fluorescence spectra of the LS films were recorded aligning the sample holder at an angle of 60° and normalized with respect to the absorbance value of the sample at 470 nm, whereas the quenching data were calculated versus the fluorescence of an equivalent sample of only P3HT.

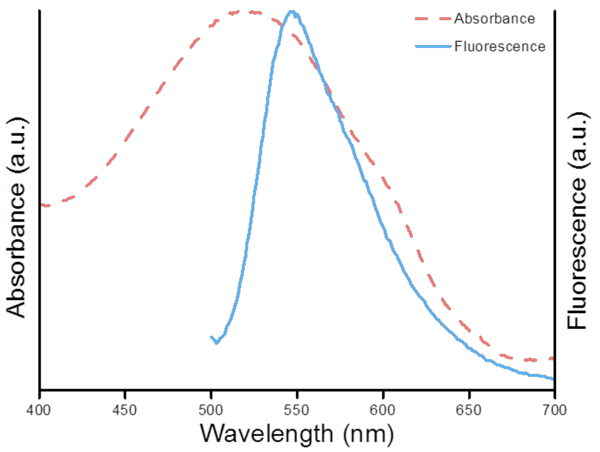

Figure S11: Overlap between the F8BT Fluorescence emission (solid line) and the P3HT UV-Vis absorption (dashed line) spectra.

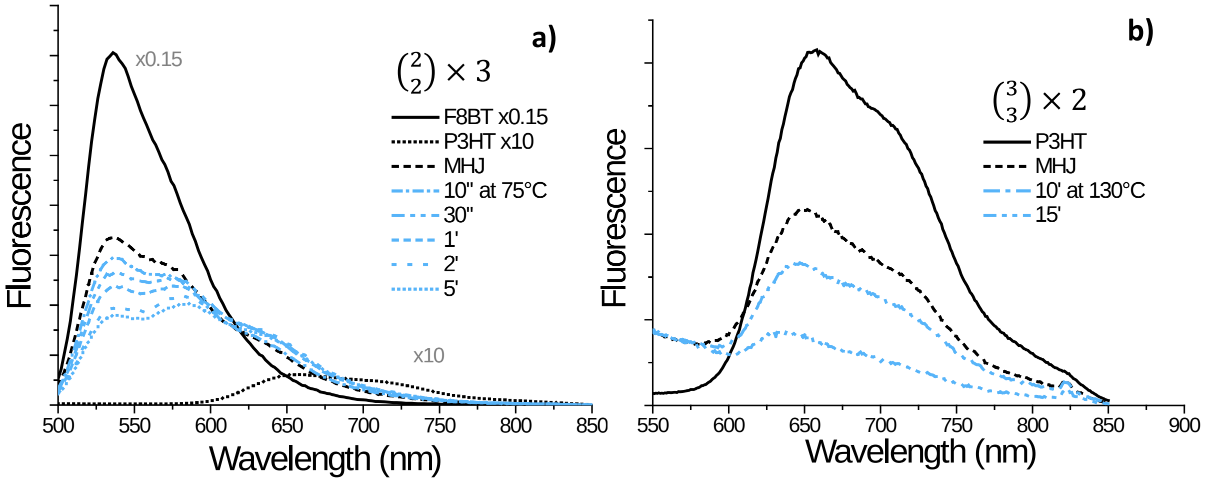

Figure S12: Fluorescence spectra of pure components and of MHJ thin-films non-annealed and at different annealing time and temperature (see legends);

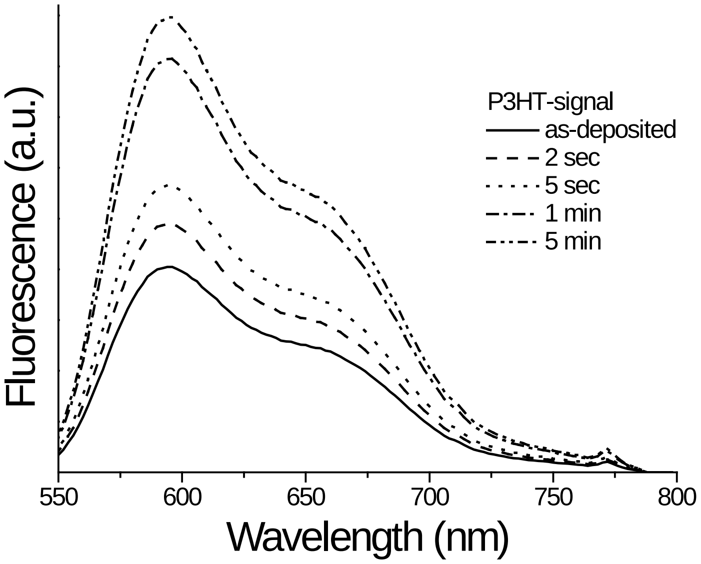

Figure S13: Fluorescence spectra of P3HT obtained by subtracting F8BT contribution from the entire spectra of a $\binom{2}{2} \times 3$ P3HT:F8BT MHJ annealed at 75°C and at different time.

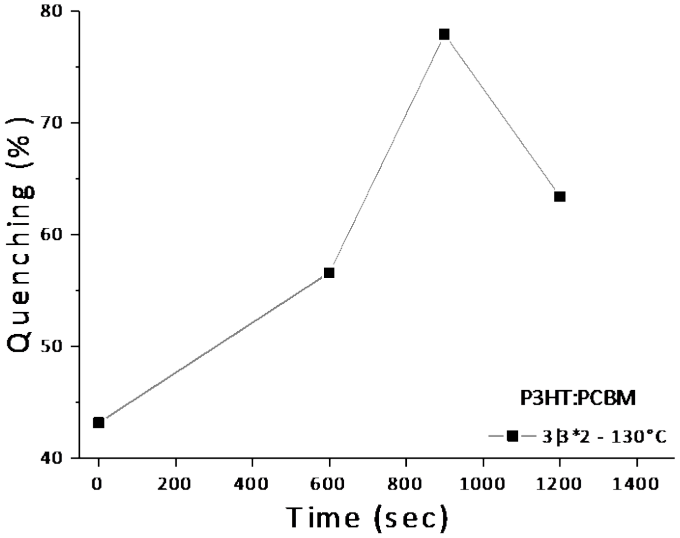

Figure S14: Quenching vs. annealing time at different temperatures for a $\binom{3}{3} \times 2$ P3HT:PCBM MHJ.

References:

1. R. J. Good and C. J. van Oss, in *Modern Approach to Wettability: Theory and Applications*, eds. M. E. Schrader and G. Loeb, Springer, New York, 1992, p. 452.
2. C. J. Van Oss, M. K. Chaudhury and R. J. Good, *Adv. Colloid Interface Sci.*, 1987, **28**, 35-64.
3. X. Qin and W. V. Chang, *J. Adhes. Sci. Technol.*, 1995, **9**, 823-841.
4. T. Hino, Y. Ogawa and N. Kuramoto, *Carbon*, 2006, **44**, 880-887.

5. F. T. Brown, *Engineering System Dynamics: A Unified Graph-centered Approach*, CRC Press, 2006.
6. E. K. Rhoderick and R. H. Williams, in *Metal-Semiconductor Contacts*, Clarendon, Oxford, 1988, ch. 1-3.
7. J. Ivanco, F. P. Netzer and M. G. Ramsey, *J. Appl. Phys.*, 2007, **101**, 103712-103717.